

## Skyrmion Qubits: A New Class of Quantum Logic Elements Based on Nanoscale Magnetization

Christina Psaroudaki<sup>1,2,\*</sup> and Christos Panagopoulos<sup>3,†</sup>

<sup>1</sup>*Department of Physics and Institute for Quantum Information and Matter, California Institute of Technology, Pasadena, California 91125, USA*

<sup>2</sup>*Institute for Theoretical Physics, University of Cologne, D-50937 Cologne, Germany*

<sup>3</sup>*Division of Physics and Applied Physics, School of Physical and Mathematical Sciences, Nanyang Technological University, 21 Nanyang Link 637371, Singapore*



(Received 30 March 2021; accepted 30 June 2021; published 4 August 2021)

We introduce a new class of primitive building blocks for realizing quantum logic elements based on nanoscale magnetization textures called skyrmions. In a skyrmion qubit, information is stored in the quantum degree of helicity, and the logical states can be adjusted by electric and magnetic fields, offering a rich operation regime with high anharmonicity. By exploring a large parameter space, we propose two skyrmion qubit variants depending on their quantized state. We discuss appropriate microwave pulses required to generate single-qubit gates for quantum computing, and skyrmion multiqubit schemes for a scalable architecture with tailored couplings. Scalability, controllability by microwave fields, operation time scales, and readout by nonvolatile techniques converge to make the skyrmion qubit highly attractive as a logical element of a quantum processor.

DOI: 10.1103/PhysRevLett.127.067201

Quantum computing promises to dramatically improve computational power by harnessing the intrinsic properties of quantum mechanics. Its core is a quantum bit (qubit) of information made from a very small particle such as an atom, ion, or electron. Proposed qubit systems include trapped atoms, quantum dots, and photons [1–3]. Among them, superconducting circuits, currently one of the leading platforms for noisy intermediate-scale quantum computing protocols [4], are macroscopic in size but with well-established quantum properties [5]. Nevertheless, despite tremendous progress, significant challenges remain, in particular with respect to control and scalability [6].

Here we propose an alternative macroscopic qubit design based on magnetic skyrmions, topologically protected nanoscale magnetization textures, which have emerged as potential information carriers for future spintronic devices [7]. We focus on frustrated magnets, in which skyrmions and antiskyrmions have a new internal degree of freedom associated with the rotation of helicity [8–12]. In these systems, the noncollinear spin texture induces electric polarization, allowing for electric-field modulation of the skyrmion helicity [13,14]. Along with magnetic field gradients [15] (MFGs) and microwave fields [16,17], electric fields emerge as a new, powerful tool for a current-free control of skyrmion dynamics [18]. Skyrmions of a few lattice sites [19] inspired theoretical studies on their quantum properties [20,21]. Similar to Josephson junctions [22,23], their macroscopic quantum tunneling and energy-level quantization are indicative of quantum behavior. In sufficiently small magnets, an analogous quantum behavior in terms of macroscopic quantum

tunneling of the magnetic moment has been experimentally verified in mesoscopic magnetic systems [24–26], while the quantum depinning of a magnetic skyrmion has been theoretically proposed [27].

We formulate a theoretical framework of skyrmion quantization and construct skyrmion qubits based on the energy-level quantization of the helicity degree of freedom. The ability to control the energy-level spectra with external parameters, including electric and magnetic fields, offers a rich parameter space of possible qubit variants with high anharmonicity and tailored characteristics. We propose microwave MFGs for skyrmion qubit manipulation and gate operation, and consider skyrmion multiqubit schemes for a scalable architecture. A skyrmion qubit has a moderately high coherence time in the microsecond regime, while nonvolatile readout techniques can be employed for a reliable qubit state readout. Finally, we discuss how scale-up multiqubit challenges can be addressed by leveraging state-of-the-art skyrmion technology and show that skyrmion qubits are suitable for quantum computing technology.

*Skyrmion field quantization.*—We begin by considering the inversion-symmetric Heisenberg model with competing interactions [10],

$$\mathcal{F} = -\frac{J_1}{2}(\nabla\mathbf{m})^2 + \frac{J_2 a^2}{2}(\nabla^2\mathbf{m})^2 - \frac{H}{a^2}m_z + \frac{K}{a^2}m_z^2, \quad (1)$$

where  $H$  and  $K$  are the Zeeman and anisotropy coupling, respectively, while  $J_1$  and  $J_2$  denote the strength of the competing interactions and  $a$  the lattice spacing. A number

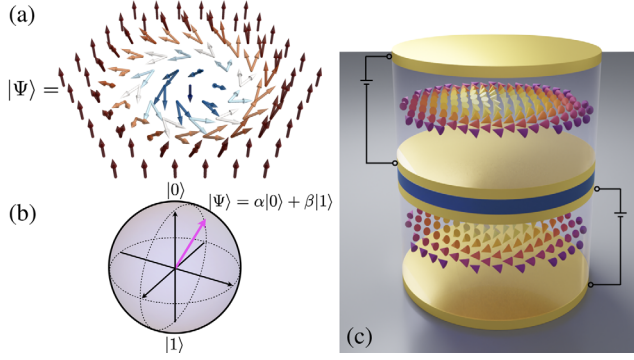


FIG. 1. Skymion qubit concept. (a) A quantum state  $|\Psi\rangle$  as an arbitrary superposition of skymion configurations with distinct helicities  $\varphi_0$ . (b) Bloch sphere representation of  $|\Psi\rangle = \alpha|0\rangle + \beta|1\rangle$ , with  $|0\rangle$  and  $|1\rangle$  denoting the two lowest energy levels of the quantum operator  $\hat{\varphi}_0$ . (c) A bilayer of magnetic materials as a platform for the skymion qubit coupling scheme. The qubit coupling is tuned by a nonmagnetic spacer (blue), and logical states are adjusted by electric fields (yellow plates).

of geometrically frustrated magnets are good candidates to host complex spin textures [8], including the triangular-lattice magnet  $\text{Gd}_2\text{PdSi}_3$ , known to support skymion phases [28]. Using  $\mathbf{m} = [\sin \Theta \cos \Phi, \sin \Theta \sin \Phi, \cos \Theta]$ , we describe classical skymions by  $\Phi(\mathbf{r}) = -Q\phi$  and  $\Theta = \Theta(\rho)$ , with  $\rho, \phi$  polar coordinates. This class of solutions is characterized by an integer-valued topological charge  $Q = (1/4\pi) \int_{\mathbf{r}} \mathbf{m} \cdot (\partial_x \mathbf{m} \times \partial_y \mathbf{m})$ , with  $Q = 1$  ( $Q = -1$ ) for a skymion (antiskyrmion). The skymion size is defined as  $\lambda \equiv 2a/\text{Re}[\gamma_{\pm}]$ , with  $\gamma_{\pm} = \sqrt{-1 \pm \tilde{\gamma}/\sqrt{2}}$  and  $\tilde{\gamma} = \sqrt{1 - 4(H/J_1 + 2K/J_1)}$ . The model of Eq. (1) has an unbroken global symmetry,  $\Phi \rightarrow \Phi + \varphi_0$ , with  $\varphi_0$  the collective coordinate of the skymion helicity. By considering a skymion stabilized in a nanodisk (see Fig. 1), we exclude the translational coordinate of position [21] and focus exclusively on the dynamics of  $\varphi_0$ .

To investigate quantum effects, we utilize a method of collective coordinate quantization. Here  $\varphi_0$  and its conjugate momentum  $S_z$  are introduced by performing a canonical transformation in the phase space path integral [29,30] (see Supplemental Material [31]). This is achieved by ensuring momentum is conserved,  $S_z = P$ , with  $P = \int_{\mathbf{r}} (1 - \cos \Theta) \partial_{\phi} \Phi$  the infinitesimal generator of rotations satisfying  $\{P, \Phi\} = -\partial_{\phi} \Phi$ . Using standard equivalence between path integral and canonical quantization, we introduce operators  $\hat{\varphi}_0$  and  $\hat{S}_z$  with  $[\hat{\varphi}_0, \hat{S}_z] = i/\bar{S}$ , and  $\bar{S}$

the effective spin. The classical limit is associated with  $\bar{S} \gg 1$ . Eigenstates of  $\hat{S}_z$  are labeled by an integer charge  $s$  with  $\hat{S}_z |s\rangle = s/\bar{S} |s\rangle$ , and states  $\hat{\varphi}_0 |\varphi_0\rangle = \varphi_0 |\varphi_0\rangle$  have a circular topology  $|\varphi_0\rangle = |\varphi_0 + 2\pi\rangle$ . The relation between physical and dimensionless parameters is summarized in Table I. We construct skymion qubits based on textures with  $Q = 1$ . Antiskyrmion qubits follow directly from our present analysis.

*Fundamental skymion qubit types.*—We now seek to construct a skymion qubit based on the energy-level quantization of the helicity degree of freedom. A promising qubit candidate needs to satisfy several criteria including scalability, ability to initialize to a simple fiducial state, long decoherence times, a universal set of quantum gates, and the ability to perform qubit-specific measurements [32].

The  $S_z$  qubit: The ability to control the energy-level spectra with external parameters, offers a rich parameter space of possible qubit variants with tailored characteristics. We introduce the  $S_z$ -qubit Hamiltonian,

$$H_{S_z} = \kappa(\hat{S}_z - h/\kappa)^2 - E_z \cos \hat{\varphi}_0, \quad (2)$$

which resembles the circuit Hamiltonian of a superconducting charge qubit [33]. Here  $\kappa$  and  $h$  denote the anisotropy and magnetic field coupling, respectively, in dimensionless units. The noncollinear spin texture gives rise to an electric polarization which couples to an electric field  $E_z$  applied across the nanodisk to control  $\varphi_0$  [14] (see Fig. 1 for a schematic illustration of the setup). The  $S_z$  qubit is designed in the  $E_z \ll \kappa$  regime, such that logical qubits are spin states  $|s\rangle$ , representing deviations of the  $m_z$  component from equilibrium. The solution of the Schrödinger equation  $H_{S_z} \Psi_s(\varphi_0) = \mathcal{E}_s \Psi_s(\varphi_0)$ , with  $\Psi_s(\varphi_0) = \langle \varphi_0 | s \rangle$ , can be calculated exactly in the form of special functions (see Supplemental Material [31]). In Fig. 2(b) we plot the potential landscape and the first three levels using  $\kappa = 0.1$ ,  $h = 0.47$ , and  $E_z = 0.02$ .

Two requirements are essential for a reliable qubit operation; nonequidistance of the energy spectrum to uniquely address each transition and suppressed spontaneous thermal excitations to higher energy levels  $k_B T \ll \hbar\omega_{12}, \hbar\omega_{02}$ . The remarkable feature of skymion qubits is that these conditions can be met by tuning the relevant external parameters. In Fig. 2(a) we present the range of parameters  $\bar{h} = h\bar{S}/\kappa$  and  $E_z$  for which a relatively large anharmonicity is present,  $|\omega_{12} - \omega_{01}| > 20\%\omega_{01}$  and  $|\omega_{02} - \omega_{01}| > 20\%\omega_{01}$ .

TABLE I. Relation between physical and dimensionless parameters. We use  $J_1 = 1$  meV,  $a = 5$  Å,  $\bar{S} = 10$ ,  $J_2 = J_1$ ,  $K = 0.4J_1$ ,  $K_x = 0.05J_1$ , and  $P_E = 20$   $\mu\text{C}/\text{cm}^2$ . MFG stands for magnetic field gradient.

Length	Time	Frequency	Temperature	Magnetic field	Electric field	Static MFG
$\mathbf{r} \times 0.5$ nm	$t \times 6.610^{-13}$ s	$\omega \times 1519$ GHz	$T \times 11.6$ K	$H/g\mu_B = h \times 0.86$ T	$E = E_z \times 215$ V/m	$H_{\perp}/g\mu_B = h_{\perp} \times 1.72$ T/nm

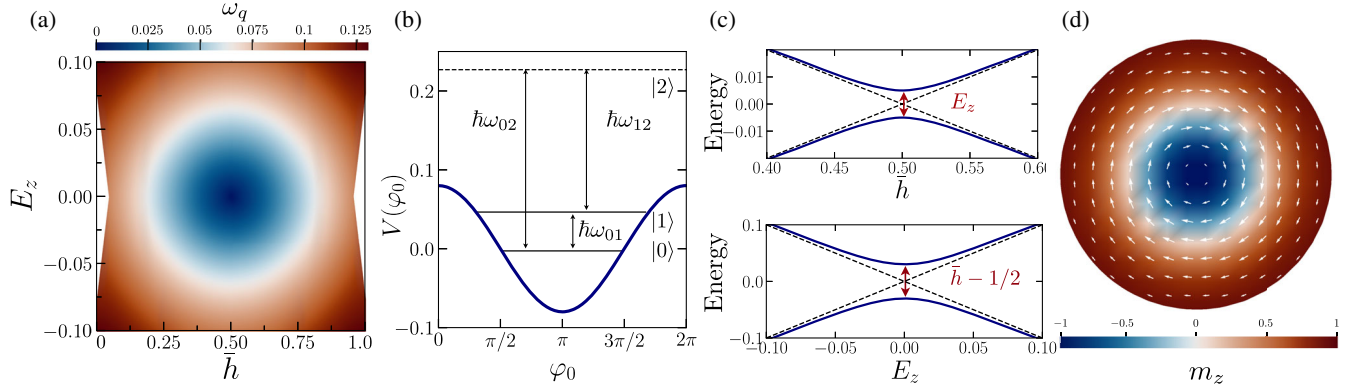


FIG. 2. The  $S_z$ -qubit properties. (a) Magnetic field  $\bar{h}$  and electric field  $E_z$  dependence of the transition frequency  $\omega_q$ , close to the degeneracy point  $\bar{h} = 0.5$ . The colored surface represents the values of  $\omega_q$  which satisfy the requirement of high anharmonicity. (b) Nonequidistant quantized energy levels and potential landscape. The qubit states are the ground state  $|0\rangle$  and first excited state  $|1\rangle$  with level spacing  $\hbar\omega_{01} = \omega_q$  smaller than transitions to higher states  $\hbar\omega_{02}, \hbar\omega_{12}$ . (c) Universal energy level anticrossing diagram close to the degeneracy point (dashed lines). The degeneracy is lifted by an electric field (upper panel) or increasing the magnetic field away from  $\bar{h} = 0.5$  (lower panel). At the degeneracy point, energy eigenstates are symmetric and antisymmetric superpositions of the skyrmion qubit states ( $|0\rangle \pm |1\rangle$ )/ $\sqrt{2}$ . (d) A magnetic skyrmion with a circular profile stabilized in a magnetic nanodisk.

For  $\bar{h} = 1/2$ , the two lowest spin states  $|0\rangle$  and  $|1\rangle$  are degenerate, and a small  $E_z$  lifts the degeneracy creating a tight two-level system. Truncating the full Hilbert space to qubit subspace, the reduced Hamiltonian is

$$H_q = \frac{H_0}{2} \hat{\sigma}_z - \frac{X_c}{2} \hat{\sigma}_x, \quad (3)$$

with  $H_0 = \kappa(1 - 2\bar{h})/\bar{S}$ ,  $X_c = E_z$ , and  $\omega_q = \sqrt{H_0^2 + X_c^2}$  the corresponding qubit level spacing. The universal level repulsion diagram is shown in Fig. 2(c), with a minimum energy splitting  $E_z$ . The  $S_z$ -qubit operation regime in physical units is given in Table II. We note that the proposed qubit platform has large anharmonicity, and the voltage bias for qubit manipulation is several orders of magnitude smaller compared to those required for the electric-field skyrmion creation and annihilation [18].

The helicity qubit: Inspired by the superconducting flux qubit and proposals on magnetic domain walls [34], we seek to construct a double-well potential landscape for the helicity  $\varphi_0$ , in order to define the qubit logical space using the two well minima. This is achieved by considering a material with in-plane magnetic anisotropy of strength  $\kappa_x$  [35] and a skyrmion characterized by an elliptical profile, as the result of defect engineering [36,37]. The Hamiltonian

for this new type of helicity qubit reads  $H_{\varphi_0} = \kappa \hat{S}_z - h \hat{S}_z + V(\hat{\varphi}_0)$ , with the double-well potential given by

$$V(\varphi_0) = \kappa_x \cos 2\hat{\varphi}_0 - E_z \cos \hat{\varphi}_0 + h_{\perp} \sin \hat{\varphi}_0. \quad (4)$$

The first two terms in Eq. (4) create a symmetric potential, and the third term describes a depth difference between the well created by an in-plane MFG of strength  $h_{\perp}$ . The solutions of the eigenvalue problem  $1H_{\varphi_0} \Psi_n(\varphi_0) = \mathcal{E}_n \Psi_n(\varphi_0)$  are  $2\pi$ -periodic functions calculated numerically. The potential in the helicity representation is schematically shown in Fig. 3(b) together with the first three levels. Close to the degeneracy point at  $\bar{h} = 1$  and for  $h_{\perp} = 0$ , the two lowest energy functions  $\Psi_{0,1}$  are symmetric and antisymmetric combinations of the two wave functions localized in each well located at  $\varphi_m = \tan^{-1}(\sqrt{16\kappa_x^2 - E_z^2}/E_z)$ . A finite  $h_{\perp}$  acts as an energy bias creating a depth well difference, such that the ground and first-excited states are now localized in different wells.

At  $\bar{h} = 1$ , level anticrossing can be probed by applying either an electric field  $E_z$  [see Fig. 3(c), upper panel] or a magnetic field gradient  $h_{\perp}$  [see Fig. 3(c), lower panel]. The

TABLE II. Skyrmion qubit operation regime and lifetime. We use  $\alpha = 10^{-5}$  and  $T = 100$  mK. EF stands for electric field and MFG for magnetic field gradient.

Qubit type	Magnetic field	External control	$\omega_q$	$T_1$	$T_2$	$\omega_{12}$	$T_c$
$S_z$ qubit	8.9 mT	EF = 108 mV/ $\mu$ m	25.6 GHz	0.27 $\mu$ s	0.49 $\mu$ s	310 GHz	2.50 K
Helicity qubit	445 mT	EF = 296 mV/ $\mu$ m	14.9 GHz	0.15 $\mu$ s	0.26 $\mu$ s	330 GHz	2.60 K
Helicity qubit	445 mT	MFG = 1.73 mT/nm	2.1 GHz	0.43 $\mu$ s	0.32 $\mu$ s	330 GHz	2.55 K

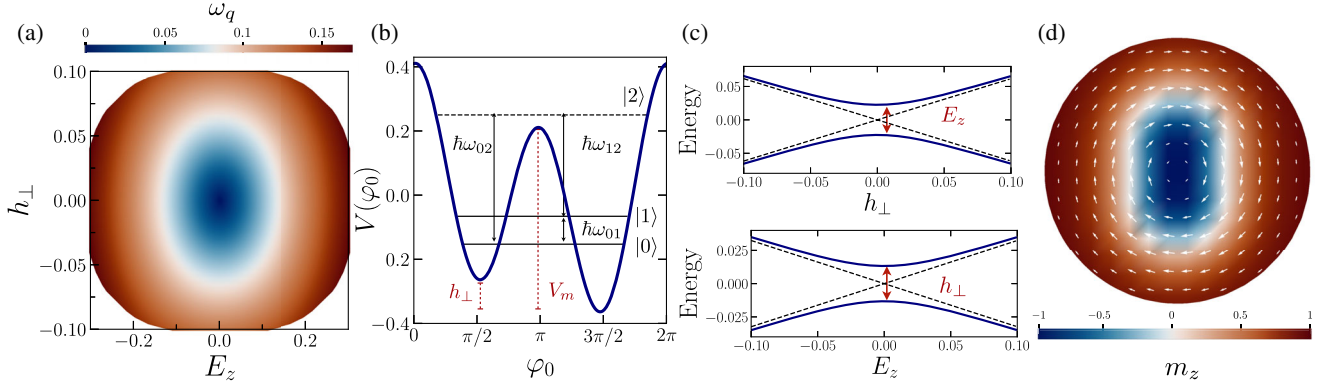


FIG. 3. The helicity-qubit properties. (a) Electric field  $E_z$  and magnetic field gradient  $h_\perp$  dependence of the transition frequency  $\omega_q$ , close to the degeneracy point  $\bar{h} = 1$ . The colored surface represents the values of  $\omega_q$  which satisfy the requirement of high anharmonicity. (b) Nonequidistant quantized energy levels and double-well potential landscape. The qubit states are the ground state  $|0\rangle$  and first excited state  $|1\rangle$  with level spacing  $\hbar\omega_{01} = \omega_q$  smaller than transitions to higher states  $\hbar\omega_{02}$ ,  $\hbar\omega_{12}$ . The potential barrier  $V_m$  is controlled by  $E_z$  and the well difference by  $h_\perp$ . (c) Universal energy level anticrossing diagram close to the degeneracy point  $\bar{h} = 1$ . The degeneracy is lifted by an electric field (upper panel) or a magnetic field gradient (lower panel). (d) A magnetic skyrmion with an elliptical profile stabilized in a magnetic nanodisk. The elliptical profile is essential for realizing the double-well potential.

reduced qubit Hamiltonian under the two-level approximation has the form of Eq. (3), where  $H_0 = \mathcal{E}_1 - \mathcal{E}_0$  and  $X_c = g_e E_z$  for  $h_\perp = 0$ , or  $X_c = g_b h_\perp$  for  $E_z = 0$ . Constants  $H_0$ ,  $g_e$ , and  $g_b$  are found numerically. The helicity-qubit operation regime in physical units is given in Table II, using both  $E_z$  and  $h_\perp$  as external control parameters.

*Qubit control.*—A quantum coherent computation depends on the ability to control individual quantum degrees of freedom. Here we propose microwave MFGs for skyrmion qubit manipulation and gate operation. MFGs give rise to additional Hamiltonian terms  $H_{\text{ext}}(t) = bf(t) \cos(\omega t + \phi_{\text{ext}}) \cos \hat{\varphi}_0$ , with  $f(t)$  a dimensionless envelope function, or in terms of the qubit Hamiltonian,  $H_{\text{ext}}^q = b_x(t) \hat{\sigma}_x$ , with  $b_x(t) = b_0 f(t) \cos(\omega t + \phi_{\text{ext}})$ . In the diagonal basis, the driven Hamiltonian is written as

$$H_q = \frac{\omega_q}{2} \hat{\sigma}_z + b_x(t) [\cos \theta \hat{\sigma}_x + \sin \theta \hat{\sigma}_z], \quad (5)$$

with  $\tan \theta = X_c/H_0$ . To elucidate the role of the drive, we transform  $H_q$  into the rotating frame,

$$H_{\text{rot}} = \frac{\Delta\omega}{2} \hat{\sigma}_z + \frac{\Omega}{2} f(t) [\cos \phi_{\text{ext}} \hat{\sigma}_x + \sin \phi_{\text{ext}} \hat{\sigma}_y], \quad (6)$$

where  $\Delta\omega = \omega_q - \omega$  is the detuning frequency and  $\Omega = b_0 \cos \theta$ . Single-qubit operations correspond to rotations of the qubit state by a certain angle about a particular axis. As an example, for  $\phi_{\text{ext}} = 0$  and  $\Delta\omega = 0$ , the unitary operator  $U_x(t) = e^{-(i/2)\vartheta(t)\hat{\sigma}_x}$  corresponds to rotations around the  $x$  axis by an angle  $\vartheta(t) = -\Omega \int_0^t f(t') dt'$  [38]. Rotations about the  $y$  axis are achieved for  $\phi_{\text{ext}} = \pi/2$ .

*Qubit coupling scheme.*—A key component for realizing a scalable quantum computer is an interaction Hamiltonian between individual qubits. As a straightforward scheme for

coupling skyrmion qubits, we consider the interlayer exchange interaction in a magnetic bilayer mediated by a nonmagnetic spacer layer (see Fig. 1 for a visualization). The interaction term is given by  $F_{\text{int}} = J_{\text{int}} \int_{\mathbf{r}} \mathbf{m}_1 \cdot \mathbf{m}_2$  [39], or in terms of the helicities,  $H_{\text{int}} = -J_{\text{int}} \cos(\varphi_1 - \varphi_2)$ . The resulting Hamiltonian in the qubit basis contains both transverse and longitudinal couplings,

$$H_{\text{int}} = -\mathcal{J}_{\text{int}}^x \hat{\sigma}_x^1 \hat{\sigma}_x^2 - \mathcal{J}_{\text{int}}^z \hat{\sigma}_z^1 \hat{\sigma}_z^2. \quad (7)$$

$J_{\text{int}}$  can be tuned experimentally by changing the spacer thickness, while both  $\mathcal{J}_{\text{int}}^{x,z}$  allow for an independent control by tuning all three external fields  $h$ ,  $E_z$ , and  $h_\perp$ . This property is especially important in applications where both longitudinal and transverse couplings are desired, such as quantum annealing [38].

*Noise and decoherence.*—The interaction of the skyrmion qubit with the environmental degrees of freedom is a source of noise that leads to decoherence. They result in Ohmic damping terms for the collective coordinates  $\varphi_0$  and  $S_z$  [40], accompanied by random fluctuating forces  $\xi_i$  that enter the quantum Hamiltonian as  $\hat{H} \rightarrow \hat{H} + \xi_{\varphi_0} \hat{\varphi}_0 + \xi_{S_z} \hat{S}_z$ .  $\xi_i$  is fully characterized by the classical ensemble averages  $\langle \xi_i(t) \rangle = 0$  and  $\langle \xi_i(t) \xi_j(t') \rangle = \delta_{ij} S_i(t - t')$  [34], and the correlator  $S_i(t)$  is defined via the fluctuation-dissipation theorem,  $S_i(\omega) = \alpha_i \omega \coth(\beta\omega/2)$ , with  $\alpha_i$  constants proportional to the Gilbert damping  $\alpha$ . In terms of the reduced qubit Hamiltonian one finds

$$H_q = \frac{\omega_q}{2} \hat{\sigma}_z + \xi_x(t) \gamma_x \hat{\sigma}_x + \xi_y(t) \gamma_y \hat{\sigma}_y + \xi_z(t) \gamma_z \hat{\sigma}_z, \quad (8)$$

where  $\gamma_i$  constants which depend on the qubit type and  $\xi_{x,y,z}$  are linear combinations of  $\xi_{\varphi_0}$  and  $\xi_{S_z}$ .

Within the Bloch-Redfield picture of two-level system dynamics, relaxation processes are characterized by the longitudinal relaxation rate  $\Gamma_1 = T_1^{-1}$  and the dephasing rate  $\Gamma_2 = T_2^{-1}$ . The latter is a combination of effects of the depolarization  $\Gamma_1$  and of the pure dephasing  $\Gamma_\phi$ , combined to a rate  $\Gamma_2 = \Gamma_1/2 + \Gamma_\phi$ , with  $\Gamma_1 = \gamma_x^2 S_x(\omega_q) + \gamma_y^2 S_y(\omega_q)$  and  $\Gamma_\phi = \gamma_z^2 S_z(0)$  [41]. The optimal regime for realizing both long coherence and high anharmonicity is close to the degeneracy point and for  $X_c \ll H_0$ . This translates to the requirement  $\hbar = 0.5$  and  $E_z \ll 1$  for the  $S_z$  qubit, and to  $\hbar = 1$  and  $E_z, h_\perp \ll 1$  for the helicity qubit.

In Table II we present the expected qubit lifetimes for a modest choice of an ultralow Gilbert damping  $\alpha = 10^{-5}$  and  $T = 100$  mK. A skyrmion qubit has a moderately high coherence time in the microsecond regime. This is comparable to early measurements of the flux superconducting qubit and 2 orders of magnitude larger than the Cooper pair box [33]. The number of coherent Rabi frequency oscillations within the coherence time is  $\Omega T_1 \propto 10^5$ , inside the desired margins expected for superconducting qubits [34,42]. Several magnetic thin films exhibit ultralow Gilbert damping of the order of  $\alpha \sim 10^{-4} - 10^{-5}$  [43–45]. In the sub-Kelvin qubit operational regime, Gilbert damping is expected to be even lower [46,47]. Coherence times can be further improved with the development of cleaner magnetic samples and interfaces in engineered architectures, without trading off qubit anharmonicity and scalability.

*Readout techniques.*—An essential part for implementing skyrmion-based quantum-computing architectures is a reliable readout. Quantum sensing of coherent single-magnon techniques, based on quantum dot [48] or superconducting qubit [49] sensors, is promising for the readout of  $S_z$ -qubit states, single magnetic excitations from the equilibrium configuration. On the other hand, helicity-qubit states represent two distinct skyrmion configurations with helicity values located at the two minima of the double-well potential of Eq. (4). Experimental observation of skyrmion helicity is possible using nitrogen-vacancy (NV) magnetometry [50], allowing for a detector-single qubit coupling control by varying the NV sensor distance from the skyrmion. Resonant elastic x-ray scattering [51] techniques provide a direct observation of skyrmion helicity, and when combined with ferromagnetic resonance measurements [52] can offer a promising single-qubit readout method. Finally, coupling a skyrmion to a magnetic force microscopy resonator allows the detection of magnetic states, which appear as resonance frequency shift signals [53].

*Conclusions.*—We proposed a novel physical qubit platform based on magnetic nanoskyrmions in frustrated magnets. The skyrmion state, energy-level spectra, transition frequency, and qubit lifetime are configurable and can be engineered by adjusting external electric and magnetic fields, offering a rich operation regime with high

anharmonicity. Microwave pulses were shown to generate single-qubit gates for quantum computing, and skyrmion multiqubit schemes were considered for a scalable architecture with tailored couplings. Whereas, nonvolatile readout techniques can be employed for a reliable qubit state readout, using state-of-the-art magnetic sensing technology. We anticipate the considerable progress in the field of skyrmionics will provide exciting new directions on the development of skyrmion qubits as promising candidates for quantum computing technology.

We thank Martino Poggio, So Takei, Daniel Loss, Ivar Martin and Markus Garst for useful discussions. C. Psaroudaki has received funding from the European Union’s Horizon 2020 research and innovation program under the Marie Skłodowska-Curie Grant Agreement No. 839004. C. Panagopoulos acknowledges support from the Singapore National Research Foundation (NRF) NRF- Investigatorship (No. NRFNRFI2015-04) and Singapore MOE Academic Research Fund Tier 3 Grant No. MOE2018-T3-1-002.

\*cpsaroud@caltech.edu

†christos@ntu.edu.sg

- [1] T. D. Ladd, F. Jelezko, R. Laflamme, Y. Nakamura, C. Monroe, and J. L. O’Brien, *Nature (London)* **464**, 45 (2010).
- [2] D. Loss and D. P. DiVincenzo, *Phys. Rev. A* **57**, 120 (1998).
- [3] M. Grimm, A. Beckert, G. Aepli, and M. Müller, *PRX Quantum* **2**, 010312 (2021).
- [4] J. Preskill, *Quantum* **2**, 79 (2018).
- [5] J. Clarke and F. K. Wilhelm, *Nature (London)* **453**, 1031 (2008).
- [6] Y. Alexeev *et al.*, *Phys. Rev. X Quantum* **2**, 017001 (2021).
- [7] A. N. Bogdanov and C. Panagopoulos, *Nat. Rev. Phys.* **2**, 492 (2020).
- [8] T. Okubo, S. Chung, and H. Kawamura, *Phys. Rev. Lett.* **108**, 017206 (2012).
- [9] A. O. Leonov and M. Mostovoy, *Nat. Commun.* **6**, 8275 (2015).
- [10] S.-Z. Lin and S. Hayami, *Phys. Rev. B* **93**, 064430 (2016).
- [11] X. Zhang, J. Xia, Y. Zhou, X. Liu, H. Zhang, and M. Ezawa, *Nat. Commun.* **8**, 1717 (2017).
- [12] A. O. Leonov and M. Mostovoy, *Nat. Commun.* **8**, 14394 (2017).
- [13] F. Matsukura, Y. Tokura, and H. Ohno, *Nat. Nanotechnol.* **10**, 209 (2015).
- [14] X. Yao, J. Chen, and S. Dong, *New J. Phys.* **22**, 083032 (2020).
- [15] A. Casiraghi, H. Corte-León, M. Vafaei, F. Garcia-Sanchez, G. Durin, M. Pasquale, G. Jakob, M. Kläui, and O. Kazakova, *Commun. Phys.* **2**, 145 (2019).
- [16] C. Psaroudaki and D. Loss, *Phys. Rev. Lett.* **120**, 237203 (2018).
- [17] Y. Okamura, F. Kagawa, M. Mochizuki, M. Kubota, S. Seki, S. Ishiwata, M. Kawasaki, Y. Onose, and Y. Tokura, *Nat. Commun.* **4**, 2391 (2013).

- [18] P.-J. Hsu, A. Kubetzka, A. Finco, N. Romming, K. von Bergmann, and R. Wiesendanger, *Nat. Nanotechnol.* **12**, 123 (2017).
- [19] R. Wiesendanger, *Nat. Rev. Mater.* **1**, 16044 (2016).
- [20] V. Lohani, C. Hickey, J. Masell, and A. Rosch, *Phys. Rev. X* **9**, 041063 (2019).
- [21] C. Psaroudaki, S. Hoffman, J. Klinovaja, and D. Loss, *Phys. Rev. X* **7**, 041045 (2017).
- [22] M. H. Devoret, J. M. Martinis, and J. Clarke, *Phys. Rev. Lett.* **55**, 1908 (1985).
- [23] J. M. Martinis, M. H. Devoret, and J. Clarke, *Phys. Rev. Lett.* **55**, 1543 (1985).
- [24] D. D. Awschalom, J. F. Smyth, G. Grinstein, D. P. DiVincenzo, and D. Loss, *Phys. Rev. Lett.* **68**, 3092 (1992).
- [25] L. Thomas, F. Lioni, R. Ballou, D. Gatteschi, R. Sessoli, and B. Barbara, *Nature (London)* **383**, 145 (1996).
- [26] J. Brooke, T. F. Rosenbaum, and G. Aeppli, *Nature (London)* **413**, 610 (2001).
- [27] C. Psaroudaki and D. Loss, *Phys. Rev. Lett.* **124**, 097202 (2020).
- [28] T. Kurumaji, T. Nakajima, M. Hirschberger, A. Kikkawa, Y. Yamasaki, H. Sagayama, H. Nakao, Y. Taguchi, T.-h. Arima, and Y. Tokura, *Science* **365**, 914 (2019).
- [29] J. L. Gervais and B. Sakita, *Phys. Rev. D* **11**, 2943 (1975).
- [30] N. Dorey, J. Hughes, and M. P. Mattis, *Phys. Rev. D* **49**, 3598 (1994).
- [31] See Supplemental Material at <http://link.aps.org/supplemental/10.1103/PhysRevLett.127.067201> for information on the considered model, the skyrmion field quantization, the construction of basic qubit types, qubit control by microwave magnetic field protocols, and details on relaxation mechanisms.
- [32] D. P. DiVincenzo, *Fortschr. Phys.* **48**, 771 (2000).
- [33] M. Kjaergaard, M. E. Schwartz, J. Braumüller, P. Krantz, J. I.-J. Wang, S. Gustavsson, and W. D. Oliver, *Annu. Rev. Condens. Matter Phys.* **11**, 369 (2020).
- [34] S. Takei and M. Mohseni, *Phys. Rev. B* **97**, 064401 (2018).
- [35] P. E. Roy, R. M. Otxoa, and C. Moutafis, *Phys. Rev. B* **99**, 094405 (2019).
- [36] I. G. Arjana, I. Lima Fernandes, J. Chico, and S. Lounis, *Sci. Rep.* **10**, 14655 (2020).
- [37] I. L. Fernandes, J. Chico, and S. Lounis, *J. Phys. Condens. Matter* **32**, 425802 (2020).
- [38] P. Krantz, M. Kjaergaard, F. Yan, T. P. Orlando, S. Gustavsson, and W. D. Oliver, *Appl. Phys. Rev.* **6**, 021318 (2019).
- [39] M. Poenar, F. Damay, C. Martin, J. Robert, and S. Petit, *Phys. Rev. B* **81**, 104411 (2010).
- [40] O. A. Tretiakov, D. Clarke, G.-W. Chern, Y. B. Bazaliy, and O. Tchernyshyov, *Phys. Rev. Lett.* **100**, 127204 (2008).
- [41] G. Ithier, E. Collin, P. Joyez, P. J. Meeson, D. Vion, D. Esteve, F. Chiarello, A. Shnirman, Y. Makhlin, J. Schrieffer, and G. Schön, *Phys. Rev. B* **72**, 134519 (2005).
- [42] M. H. Devoret and R. J. Schoelkopf, *Science* **339**, 1169 (2013).
- [43] L. Soumah, N. Beaulieu, L. Qassym, C. Carrétéro, E. Jacquet, R. Lebourgeois, J. Ben Youssef, P. Bortolotti, V. Cros, and A. Anane, *Nat. Commun.* **9**, 3355 (2018).
- [44] C. Guillemard, S. Petit-Watelot, L. Pasquier, D. Pierre, J. Ghanbaja, J.-C. Rojas-Sánchez, A. Bataille, J. Rault, P. Le Fèvre, F. Bertran, and S. Andrieu, *Phys. Rev. Applied* **11**, 064009 (2019).
- [45] B. Heinrich, C. Burrowes, E. Montoya, B. Kardasz, E. Girt, Y.-Y. Song, Y. Sun, and M. Wu, *Phys. Rev. Lett.* **107**, 066604 (2011).
- [46] H. Maier-Flaig, S. Klingler, C. Dubs, O. Surzhenko, R. Gross, M. Weiler, H. Huebl, and S. T. B. Goennenwein, *Phys. Rev. B* **95**, 214423 (2017).
- [47] A. Okada, S. He, B. Gu, S. Kanai, A. Soumyanarayanan, S. T. Lim, M. Tran, M. Mori, S. Maekawa, F. Matsukura, H. Ohno, and C. Panagopoulos, *Proc. Natl. Acad. Sci. U.S.A.* **114**, 3815 (2017).
- [48] D. M. Jackson, D. A. Gangloff, J. H. Bodey, L. Zaporiski, C. Bachorz, E. Clarke, M. Hugues, C. Le Gall, and M. Atatüre, *Nat. Phys.* **17** (2021), 585.
- [49] D. Lachance-Quirion, S. P. Wolski, Y. Tabuchi, S. Kono, K. Usami, and Y. Nakamura, *Science* **367**, 425 (2020).
- [50] Y. Dovzhenko, F. Casola, S. Schlotter, T. X. Zhou, F. Büttner, R. L. Walsworth, G. S. D. Beach, and A. Yacoby, *Nat. Commun.* **9**, 2712 (2018).
- [51] S. L. Zhang, G. van der Laan, W. W. Wang, A. A. Haghighirad, and T. Hesjedal, *Phys. Rev. Lett.* **120**, 227202 (2018).
- [52] S. Pöllath, A. Aqeel, A. Bauer, C. Luo, H. Ryll, F. Radu, C. Pfléiderer, G. Woltersdorf, and C. H. Back, *Phys. Rev. Lett.* **123**, 167201 (2019).
- [53] E. Marchiori, L. Ceccarelli, N. Rossi, L. Lorenzelli, C. L. Degen, and M. Poggio, [arXiv:2103.10382](https://arxiv.org/abs/2103.10382).